PHOTEK
ENVISAGE THE FUTURE

Technical Note – Characterization of an Intensified Gd_2O_2S sCMOS Neutron Camera

PRELIMINARY

Abstract

Neutron Imaging is a steadily expanding area of imaging technology with increasing interest from applications such as cultural heritage, palaeontology, and metallurgy. Increased demand for access combined with a limited number of suitable beamlines requires efficient use of available beamtime. N-Cam is a new experimental thermal and cold neutron camera system designed with increased sensitivity, thus able to capture detailed images with reduced exposure time as compared to most neutron cameras. N-Cam utilizes a 20µm thick Gd_2O_2S:Tb (Gadox) scintillator applied directly onto the input window of an image intensifier. In experiments performed at the Rutherford Appleton Laboratory ISIS-IMAT facility, N-Cam demonstrated good contrast imaging with 10 lp/mm spatial resolution in 5 second exposures over a 75mm field of view (FOV). The Modular Transfer Function (MTF) was calculated at multiple positions to assess the direction dependence of spatial resolution. Edge effects were observed in both directions but more strongly pronounced in the Y direction. A contrast phantom was used to measure 350 grey scales over a spatial scale of several mm in 600s at a neutron flux of $2x10^7$ n/cm^{2}s. The Detective Quantum Efficiency (DQE) of the system is estimated to be 16% based on analysis of flat field images.

Introduction

Neutron Imaging is a continually developing form of Non-Destructive Testing (NDT or NDE) which has seen significant interest in recent years. Several imaging techniques exist which are frequently used by industries such as automotive and aerospace as well as academia [1, 2, 3]. Neutron Imaging is steadily becoming a standard technique as more facilities become capable and interest in the technique grows.

Neutron Imaging is often compared to X-ray Imaging. This is because the two techniques are very similar, differing on how the ionizing radiation is produced and attenuated [3, 4]. X-rays interact with the electron cloud of materials and are attenuated by denser materials or heavier elements. Neutrons interact with the nucleus and attenuate faster with lighter elements. Multiple techniques have developed in neutron imaging including stroboscopic, energy selective, and 3D tomography.

One of the main limitations of neutron imaging as an NDT technique is the accessibility and cost of well collimated neutron sources with a high flux. In the last decade, there has been a push to make neutron imaging more accessible to industry and academics [3, 4, 5, 6]. These include coordinated research projects, funding to improve research reactors and their capabilities, and introducing the technique to new industries. The development of the Intensified Gadox sCMOS Neutron Camera (N-Cam) increases the accessibility to neutron facilities through its high sensitivity resulting in faster image integration times while maintaining excellent spatial resolution. It also provides opportunities for lower flux reactors to provide neutron imaging services as less flux is required to produce an image. The IMAT facility at the ISIS Neutron and Muon source provides a relatively stable beam with a large neutron flux at the sample location [7]. This was used to characterize the performance of N-Cam whilst in different operating modes.

Experiment & Analysis Methodology

Detector

The N-Cam detector comprises a 7.3 mg/cm^2 Gadox scintillator with nominal 20 µm thickness and 75 mm diameter active area. The inside of a 1.0 mm thick blackened Aluminum cover was placed 2.7 mm in front of the Gadox resulting in a minimum distance of 3.7 mm between test objects and the Gadox scintillator. The Gadox was applied directly to the fiber optic input window of a Photek MCP175 Image Intensifier. The Numerical Aperture (NA) 1,0 fiber optic input ensured high collection efficiency of the Gadox light emission. A typical neutron interacting in the scintillator deposited about 30 keV of energy via the resulting Internal Conversion Electrons (ICE,) [8] [9] [10] producing about 1200 photons accounting for the average electron pathlength in the scintillator. Roughly 32% of this light was transmitted through the fiber optic window to the photocathode. For this test the N-Cam GADOX was configured without a reflective cover layer to maximize spatial resolution, at a sacrifice of some light collection. An S-20 photocathode deposited on the inside surface of the fiber optic window provided about 10 % quantum efficiency at the peak Gadox emission of 545 nm. The resulting signal generated in the Intensifier was about 38 photoelectrons per absorbed neutron that resulted in an ICE. These photoelectrons were accelerated over a 300 µm gap at a voltage of +200V between the photocathode and microchannel plate (MCP.) The MCP is a thin glass plate with millions of pores that are used to amplify the electronic signal [11]. The N-Cam was configured with an MCP having 12 µm diameter pores on a pitch of 15 µm, and a pore Length-to-Diameter (L:D) ratio of 60:1. The MCP gain was controlled by the voltage applied across the MCP, for most of the test set to +900 V. The amplified electrons leaving the MCP were accelerated to 5.5 kV and impacted a P46 phosphor on the inside surface of the Intensifier's glass output window. The total light gain of the Intensifier at the above voltages was 10^4.

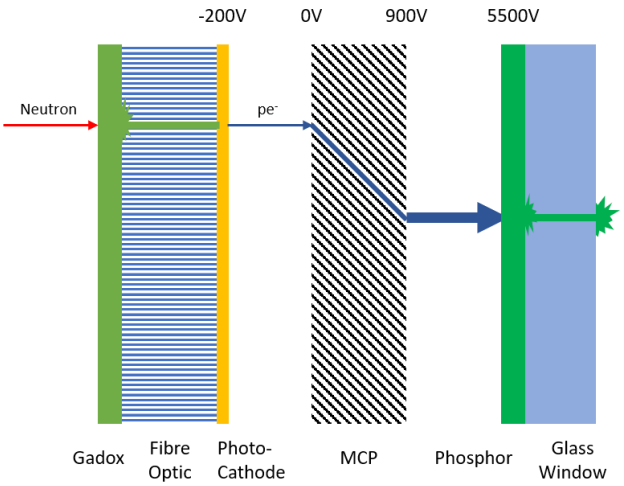

Figure 1: Diagram of a Photek Intensifier Tube

The High Voltage Power Supply (HVPS) and Intensifier Gate Control Unit (GCU) were mounted inside the camera enclosure and shielded from neutrons by two layers of 3.2 mm thick Shieldwerx Flexi-Boron shielding. A Photek HVPS with integral 50 ns gate pulse was controlled by the GCU. The photocathode voltage can be gated OFF by a -50V bias on the photocathode to MCP voltage, preventing photoelectrons from being amplified in the intensifier. The intensifier can be gated on or off on timescales of 50 ns to enable energy selective imaging. The GCU, connected by an USB interface to a Data Acquisition and control computer (DAQ), controlled the MCP voltage, Photocathode ON/OFF, Gate Duration, and Gate Delay. A signal provided by IMAT was used to synchronize the GCU with the start of the neutron beam for several acquisition modes.

Detector Readout

The camera portion of the N-Cam system is based on the Tuscen Dhyana 400D cooled sCMOS camera having 6.5 µm square pixels in a 2048x2048 array format. The maximum full-frame frame rate is 35 frames per second (fps) and can be higher with pixel binning and ROI selection. For this experiment the frame rate was varied between 0.1 and 30 fps. The full well capacity of 30,000 electrons, read noise < 2 electrons, and 16-bit digitization provided excellent dynamic range. Dark current and fixed pattern noise were minimized by cooling to -15 °C throughout the experiment. Connection to the DAQ was by a single USB3.0 interface. The camera was controlled using the Tucsen Mosaic software package.

A 45-degree front-surface mirror was used to direct the image intensifier light to the camera, mounted at 90 degrees to minimize exposure to the neutron beam. As a further precaution two layers of 3.2 mm thick Shieldwerx Flexi-Boron neutron shielding were placed in front of the camera to minimize single event upsets, radiation damage, and activation. The full 75mm detector FOV was imaged onto the camera sCMOS sensor with a Schneider-Kreuznach Componon 2.8/40 lens. The camera was mounted on a translation stage used for fine focus. During part of the experiment the camera was moved forward with an extra a lens extension ring to obtain an estimated 33 mm FOV resulting in an effective pixel size of 16.3 µm.

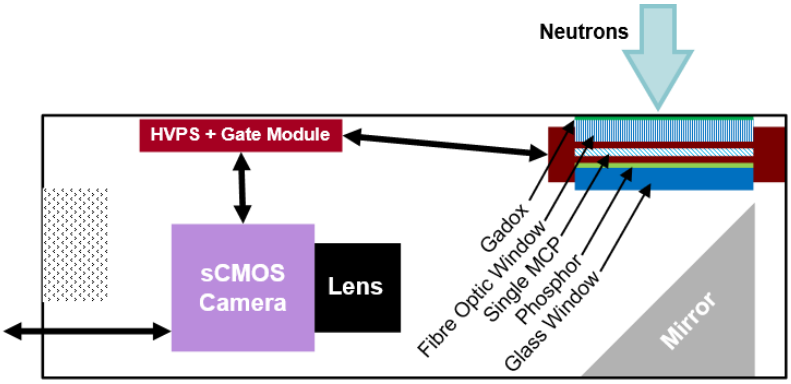

Figure 2: Diagram of N-Cam with labelled components

Image Processing

The recorded images were processed using ImageJ software. For each dataset, a mean dark field, flat field, and object image were compiled. First, a mean background image was calculated from the entire stack of background images. To estimate the mean flat field, the mean background was subtracted from every flat field image. The resultant background subtracted flat field stack was then normalized and averaged, producing the mean flat field. To generate the object image, the image stack was background subtracted, normalized, and divided by the mean flat field. The exposure time of the camera was varied by adjusting the size of the object stack. By dividing the mean object image by the flat field, gain variations and fixed pattern noise are minimized [7, 12]. The resulting final images were used in further analysis.

$$\textit{Equation 1:} \quad Normalised\ Image = \frac{Raw\ Image - Dark\ Field}{Flat\ Field - Dark\ Field}$$

Spatial Resolution

To determine the limiting spatial resolution of the neutron camera system, images were recorded of a resolution chart procured from the Paul Scherrer Institute (PSI). The PSI chart contained 3 sets of decreasing sizes of line pairs (200–1000µm, 25–150µm, 5–25µm) and a 3° tilted box for analysis of modular transfer function (MTF). The limiting resolution of both 75mm and 30mm FOV were assessed.

For the 75mm FOV, the IMAT pinhole was set to 40mm, producing an estimated neutron flux of $5x10^6$ n/cm^2/s and 245:1 L:D at the sample. A series of 60 flat field and 60 background frames were recorded at 0.2 FPS for a total exposure time of 300s each. The resolution chart was attached to the front of the intensifier at the center where 60 frames were recorded. To assess any XY dependency, the resolution chart was also placed along the edge at 3, 6, 9, and 12 o'clock positions on the intensifier, collecting an additional 60 frames at each position. For the 30mm FOV, 30 frames were recorded over 300s for both the flat field and the resolution chart, which was attached only to the center of the intensifier.

Once the images were processed, multiple line profiles were drawn across the first and second group of line pairs (25–1000µm). For each size of line pairs, the contrast was calculated using Equation 2. To calculate an the MTF curve of the image, an ImageJ plugin was utilized where the region of interest was defined around the tilted box.

$$\textit{Equation 2:} \quad Contrast = \frac{I_{peak} - I_{min}}{I_{peak} + I_{min}}$$

Sensitivity

The sensitivity of a scintillator-based neutron imager can be difficult to assess. By first principles the external Quantum Efficiency (QE) of the scintillator screen is

$$\textit{Equation 3:} \qquad QE = \eta_{nc}\,\eta_{ice}$$

where η_{nc} is the neutron capture probability and η_{ice} is the probability of a capture event generating an ICE. For the Gadox scintillator used in these measurements about 85% of neutrons undergo neutron capture and about 55% of these result in an ICE, giving a theoretical maximum QE of about 47%. The capture probability was calculated using the NIST neutron activation and scattering calculator [13] and the IMAT single frame white beam energy spectrum from Kochelmann et al [7].

In practice the DQE is less than the QE due to effects such as detector non-uniformities, light collection efficiency, and the wide variation of energy deposition per ICE and therefor light yield within the scintillator. Energy depositions can vary from nearly 0 keV for ICE which are produced at the surface of the scintillator and escape to > 100 keV for the highest energy ICE which travel in the plane of the scintillator. Here we attempt to estimate DQE by analyzing frames exposed to the full white beam while accounting for light spreading within the detector system that results in correlations between nearby pixels leading to over-estimation of DQE for small pixel sizes. For a field with uniform neutron flux yielding an average pixel signal of μ_{FF}, we expect the standard deviation of pixel values, σ_{FF}, over a modest region of the detector to be dominated by Poisson statistics of the ICE generating neutrons within that area, parameterized as:

$$\textit{Equation 4:} \qquad \frac{\sigma_{FF}}{\mu_{FF}} = \frac{1}{\sqrt{N(x)}} \cong \frac{1}{\sqrt{DQE \times F_N \times T \times (x + 2r)^2}}$$

where N(x) is the number of neutrons contributing to signals in a pixel of size x, F_N is the neutron flux in units of n/cm^{2}s, T is the integration time, and r is the correlation scale length in cm and can be thought of as the radius of light generated by a neutron. Different pixel sizes are obtained by binning the flat field data and subsequent fitting of equation 4 provides an estimate of both DQE and r. Flat field data with the IMAT beam configured with the 80 mm pinhole, flux of 2 x 10^7n/cm^{2}s, was obtained at the standard image intensifier settings and 1 s frame integration time. A flat field reference image was generated using 150 frames of data from a continuous run and a 5-frame signal image was obtained from data immediately prior to the reference image. The data was normalized and flat field corrected as given by equation 1.

Contrast to Noise

Contrast-to-Noise (CNR) is a measure of the grayscale resolution of an imaging system. To measure this a contrast phantom was fabricated using 10 thicknesses each of C101 Copper and 6082-T651 grade Aluminum, from 5 mm through 14 mm in 1 mm increments. Each section of the phantom was 5 mm x 5 mm in cross-section. The phantom was imaged using the IMAT 80 mm pinhole beam-line configuration with a nominal neutron flux of 2 x 10^7 n/cm^{2}s and L:D of 125:1. The camera was configured for one second integrations, resulting in about 50% of maximum well capacity. The image intensifier was configured with an MCP voltage of 900V and screen voltage of 5500V. Two sets of flat field images were taken before and after the contrast phantom, each consisting of 300 one second integrations. A single set of 300 one second integration background images were obtained immediately following the initial flat field sequence with the IMAT beam off and the fast beam attenuator in place. A single set of 600 one second integration images were obtained with the contrast phantom mounted directly to the input cover of the camera.

Image processing of all flat field and background images included background subtraction, conservative bright and dark pixel substitution, and normalization using a 39,872 pixel region of the camera immediately above the location of the contrast phantom to correct for beam intensity and gain variability over the exposure period. The resulting image showed non-uniformity near the edges of each of the 20 contrast sections, assumed to be due to edge effects including beam divergence and neutron scattering and diffraction along the sharp boundaries between each section of the phantom. For each 5 mm square section of the contrast phantom a 32 x 64 pixel ROI was selected near its center and the mean and standard deviation of pixel values calculated. The CNR between two adjacent sections, A and B, is defined as

$$\textit{Equation 5:} \quad CNR = \frac{|\, I_A - I_B \,|}{\sqrt{\sigma_A^2 + \sigma_B^2}}$$

Results & Discussion

Spatial Resolution

Figure 3 shows the processed images (with 300s exposure time) of the resolution chart in the center for 75mm and 33mm FOV. Using the line profiles measured in ImageJ, we estimate the limiting (5%) resolution of N-Cam to be 12.5 lp/mm and 10 lp/mm for the 30mm and 75mm FOV respectively. For the 75 mm FOV having a pixel size of 38 µm, the Nyquist limit is 13 lp/mm. When combined with the 16 lp/mm resolution of the MCP175 this agrees well with the measured 10 lp/mm. For the 33 mm FOV data with 16 µm pixels, the Nyquist limit is 30 lp/mm and combined with the 16 lp/mm of the image intensifier is consistent with the measured 12.5 mm, although we cannot rule out other limitations beginning to impact the 33 mm FOV data. A more detailed measurement would be required to determine the impact of the scintillator screen for example.

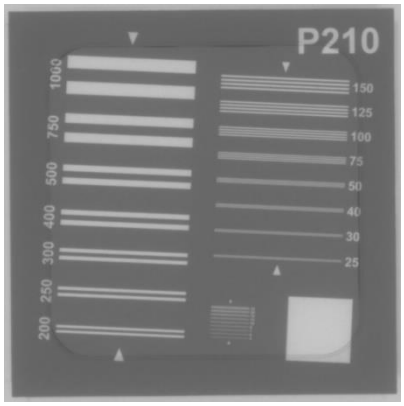

(a) Resolution chart in center (75mm FOV)

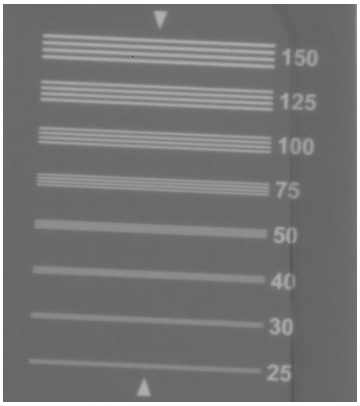

(b) Resolution chart (75mm FOV) with line widths 25-150µm

Figure 3: Processed neutron radiographs of PSI resolution chart

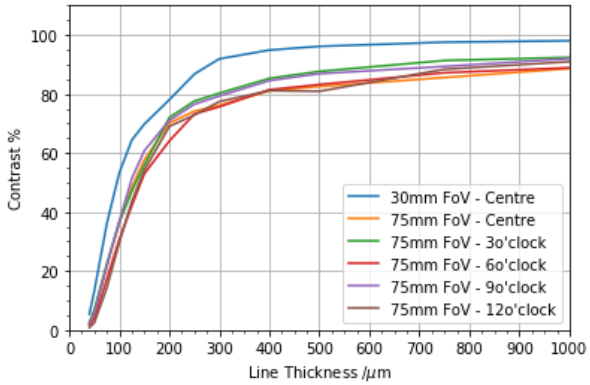

Figure 4: Mean measured contrast of different sized line pairs

Decreasing the exposure time from 300s to 30s does not affect the measured contrast or calculated MTF curve as seen in Figure 5. Decreasing the exposure time below 30s, the trend of the measured contrast and calculated MTF curves are the same but more noise is introduced, as seen in Figure 6. However, the point at which the MTF curve is less than 5% remains between 9.5 – 10.5 lp/mm.

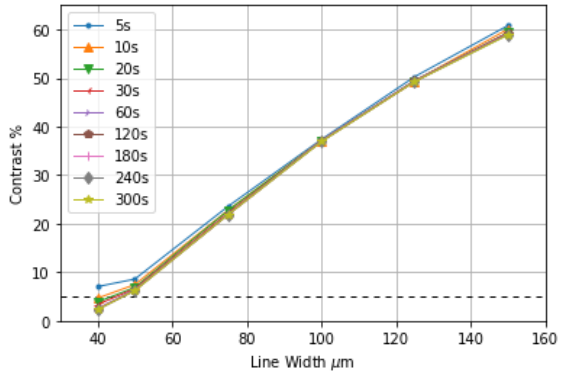

Figure 5: Measured contrasts for 75mm FoV as function of line width

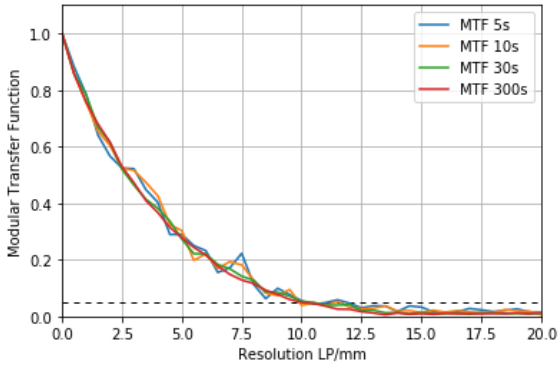

Figure 6: Calculated MTF curves of 75mm FoV for 5s, 10s, 30s, and 300s exposure time

By assessing the mean contrast at different positions, a small x and a noticeable y variation can be identified, as seen in Figure 4. Notably, while there is a small variation of the mean contrast in the X direction of 1.1%, there is a 3.7% variation in the Y direction. This XY dependence is also observed in the calculated MTF curves as seen in Figure 7. This could be due to several factors and needs to be investigated further. The final calculated MTF curves, Figure 8, were calculated by taking the mean of the X and Y MTF curves at the center.

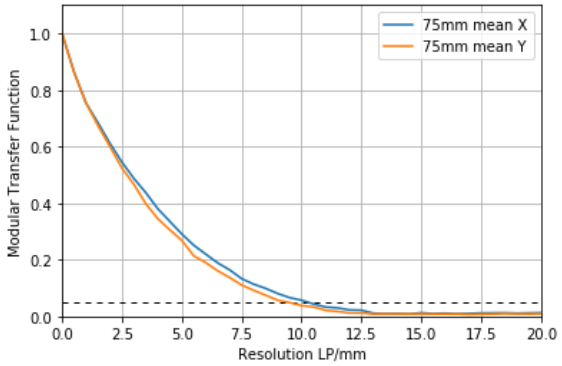

Figure 7: Mean calculated MTF curve of resolution chart in X and Y direction

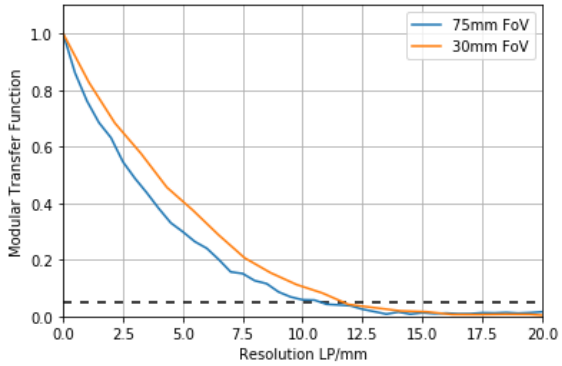

Figure 8: Mean calculated MTF curves at the center of N-Cam FoV

Evaluation for image retention was also performed by dividing before and after flat fields. After adjusting the contrast of the image, a slight outline of the resolution chart edges could be observed. By measuring line profiles across the area, a drop in mean intensity from 1.014 to 1.011 could be observed. As this represents a drop of 0.3% over the course of 2.5 hours and assuming a linear relationship, it was deemed negligible.

Detective Quantum Efficiency

The factional standard deviation of a 24 mm x 24 mm region in a flat field corrected image is given as a function of pixel size in Figure 9, where T = 5 s and $F_N = 2 \times 10^7$ n/cm^{2}s, and have been corrected for Poisson noise contributions from the 150 s image used for the flat field correction. The data are well fit with Equation 4, resulting in an estimated DQE = 16.1% and r = 81 µm. While the DQE is lower than the theoretical value of 47%, this is accounted for by a combination of low energy loss ICE near the surfaces of the Gadox layer and the broad pulse height distribution of the Gadox scintillator, as well as other non-uniformities and noise sources throughout the detector chain. The value of r = 81 µm indicates that neutron interactions that distance from the edge of a pixel will make a meaningful contribution to the signal detected in that pixel. This is not surprising given the amount of light scatter within particle-based phosphor screens, and is consistent with the MTF measurements above, where the 50% contrast is at 2.5 lp/mm, or line widths of 200 µm, roughly equal to 2r. Alternative methods of applying the Gadox screen will be investigated to determine their impact on r and the limiting resolution of the system.

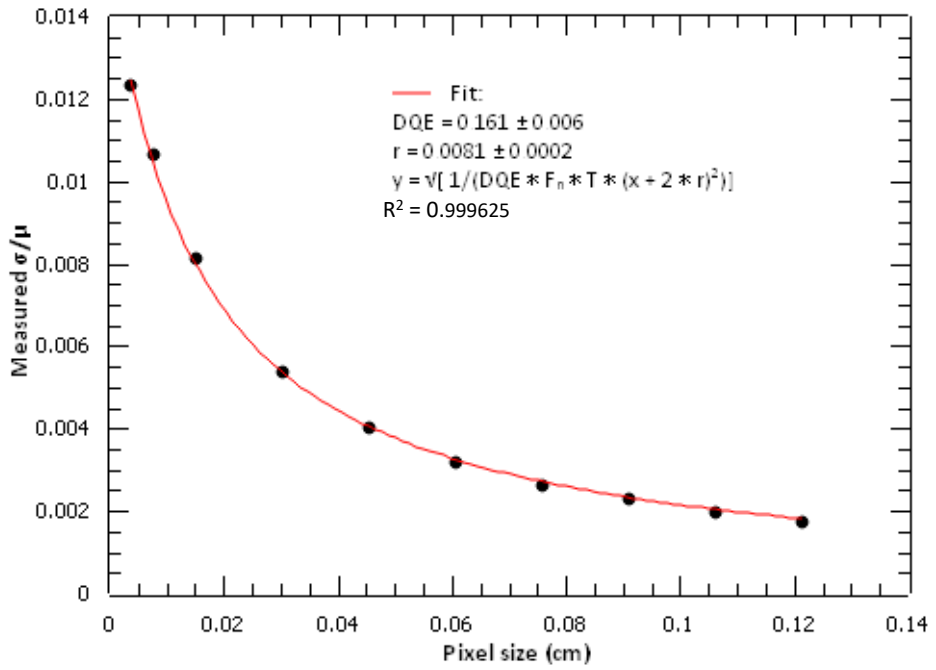

Figure 9: Fit to standard deviation as a function of pixel size using Equation 4, parameterized with QE_{eff} and r.

Contrast to Noise

Images of the flat field corrected contrast phantom are given in Figure 10 for the full 600 s image sequence. Construction of the phantom can be seen in Fig 10b, consisting of four step-wedge pieces and an Aluminum holder with two Titanium screws. The active region of each step wedge is 5 mm wide x 25 mm long, with thicknesses varying from 5 mm to 9 mm in one wedge of each material and 10 mm to 14 mm in the second wedge, each step 5 mm long. The copper step-wedges are on the left of the image with an enlargement in figure 10a. The aluminum step-wedges are on the right of the phantom with an enlarged image in figure 10c.

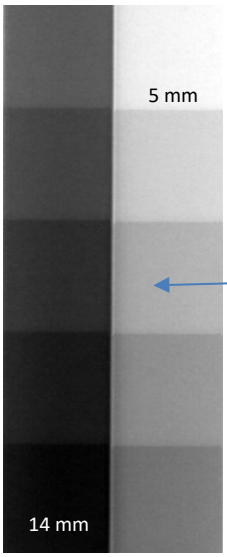

10a) Copper step-wedge from 5 to 14 mm in 1 mm steps

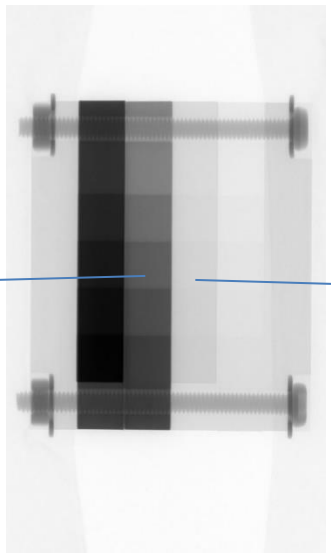

10b) Contrast Phantom

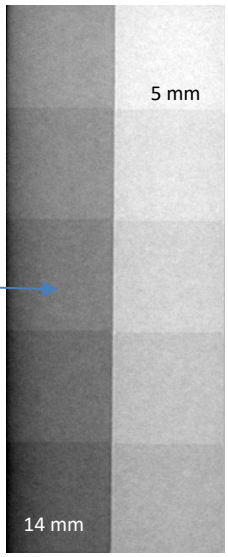

10c) Aluminum Step-wedge from 5 to 14 mm in 1 mm steps

Figure 11 shows the measured transmission for each step along with the associated noise level. From this data the CNR between the 1.0 and 1.1 cm thick Aluminum sections is found to be 2.6 and for the same copper sections the CNR is 11.4. Assuming that a CNR of 1.0 is the minimum detectable contrast we find for the aluminum data that the minimum contrast detectable is about 0.26% and the minimum detectable contrast for the copper data is about 0.30%, indicating that there are roughly 350 gray scales in the image. This value is dependent on characteristics of the neutron beam, and both sample composition and geometry.

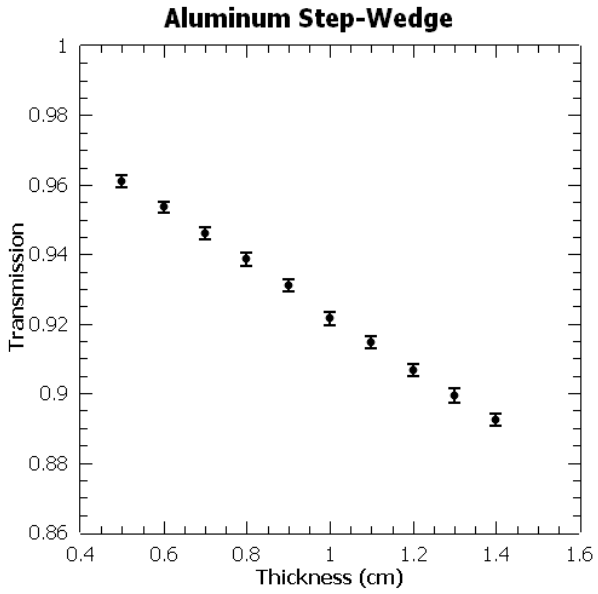

Figure 11a. Transmission through the aluminum step-wedge with error bars representing 1 σ noise.

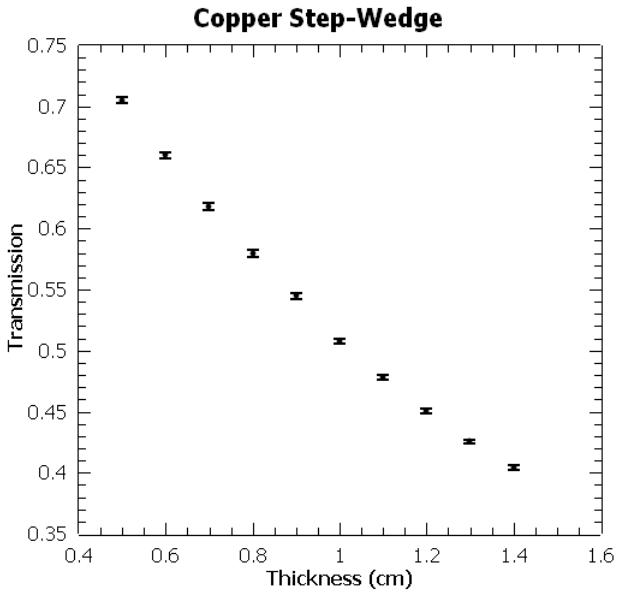

Figure 11a. Transmission through the copper step-wedge with error bars representing 1 σ noise.

Conclusion

N-Cam demonstrates 10 lp/mm resolution with 75mm field of view and 300s exposure time. Decreasing the exposure time to 30s has little effect on the observed resolution. Decreasing the exposure time below 30s, N-Cam maintains a 10 lp/mm resolution although experiences lower a signal-to-noise ratio. Therefore, assuming a 300s flat field, 300s dark field, and 360 rotations, a tomograph could be as fast a 40mins with 5s radiographs or 3 hours with 30s radiographs. N-Cam does display a direction dependence between the X & Y directions. While the X dependence could be disregarded, the Y dependence is consequential. The cause of dependence needs to be determined. The investigation into the DQE of 16.1% suggests that the scintillator thickness may affect the limiting spatial resolution of N-Cam for smaller FOV configurations and will be investigated in the future. However, the impact on the 75 mm FOV resolution is negligible which is currently limited by pixel size.

References

[1] E. Lehmann, "Neutron Imaging Facilities in a Global Context," *Journal of Imaging,* vol. 3, no. 52, pp. 1-11, 2017.

[2] B. Schillinger et al, "Neutron Imaging in Cultural Heritage Research at the FRM-II Reactor of the Heinz Maier-Leibnitz Center," *Journal of Imaging,* vol. 4, no. 22, p. 1–11, 2018.

[3] E. Lehmann et al, "Recent Application of Neutron Imaging Methods," *Physics Procedia,* vol. 88, pp. 5-12, 2017.

[4] E. Lehmann et al, "Status and Perspectives of Neutron Imaging Facilities," *Physics Procedia,* vol. 88, pp. 140-147, 2017.

[5] IAEA, Neutron Imaging as an NDT Tool, 2008.

[6] IAEA, "Neutron Generators for Analytical Purposes," 2012.

[7] W. Kochelmann et al, "Time-of-Flight Neutron Imaging on IMAT@ISIS: A New User Facility for Material Science," *Journal of Imaging,* vol. 4, no. 47, pp. 1-22, 2018.

[8] A. A. Harms and G. McCormack, "Isotopic Conversion in Gadolinium Exposure Neutron Imaging," *Nuclear Instruments and Methods,* vol. 118, pp. 583-587, 1974.

[9] P. Kandlakunta et al, "Measurement of Internal Conversion Electrons from Gd Neutron Capture," *Instrument and Methods in Physics Research A,* vol. 705, pp. 36-41, 2013.

[10] NIST, "ESTAR Stopping Power and Range Tables for Electrons," 2020. [Online]. Available: https://physics.nist.gov/PhysRefData/Star/Text/ESTAR.html.

[11] J. L. Wiza, "Microchannel Plate Detectors," *Nuclear Instrumentation & Methods,* vol. 162, p. 587–601, 1979.

[12] B. Schillinger, "An Affordable Image Detector and Low Cost Evaluation System for Computed Tomography using Neutrons, X-Rays, or Visible Light," *Quantum Beam Science,* vol. 3, no. 21, p. 1–13, 2019.

[13] NIST NCNR, "Neutron Activation and Scattering Calculator," 2020. [Online]. Available: https://www.ncnr.nist.gov/resources/activation/.